



Real-time monitoring of the pH of white wine and beer with colorimetric sensor arrays (CSAs)

Andrea Pastore, Denis Badocco, Luca Cappellin, Mauro Tubiana, Paolo Pastore*

Department of Chemical Sciences, University of Padua, Via Marzolo 1, 35131 Padua, Italy

ARTICLE INFO

Keywords:

Colorimetric sensor arrays
Wine
Beer
pH measurement
Chemical sensors
Real-time monitoring

ABSTRACT

The real-time monitoring of the pH values of alcoholic beverages was performed with a compact wireless device based on a colorimetric detection method with the Hue (H) as the analytical signal working in a pH range of 2.50–6.50. This device represents the first colorimetric pH meter reported in the literature monitoring in real-time the pH value of colored solutions. This pH meter consists of I) a nitrocellulose membrane impregnated with a pH-sensitive gel; II) a CCD camera for color acquisition; III) an electronic board with the calibration profiles of H vs. pH, and IV) a display to read the measured pH. It was applied to the pH determination of a white wine, a prosecco white wine, and a double malt beer leading to the values of $pH_{\text{wine}} = 3.30$, $pH_{\text{prosecco}} = 3.33$, $pH_{\text{beer}} = 4.29$. The analytical performance is comparable to the glass electrode with an accuracy error ≤ 0.05 pH units.

1. Introduction

The real-time monitoring of the pH of fermented beverages like wine and beer is paramount to taking control of the various stages of fermentation and aging (Markoski, Garavaglia, Oliveira, Oliveira, & Marcadenti, 2016). For this reason, the development of a stable and robust pH sensor is desirable (Magnaghi et al., 2023). The glass electrode can be used primarily for batch measurements and it requires frequent calibration and is characterized by an error of at least 0.02 pH units (Belyustin & Ivanovskaya, 2021; Salis et al., 2006; Stoica, Anes, Fiscaro, & Camões, 2021). In winemaking, the appropriate management of acidity determines the quality of wines (Giménez-Gómez et al., 2016). The pH of wine is closely linked to its microbiological and physicochemical stability (Comuzzo & Battistutta, 2018). The pH value is related to the outset of the malolactic fermentation (Cinquanta, De Stefano, Formato, Niro, & Panfili, 2018; Pacheco, Winckler, Marin, Perrier-Cornet, & Coelho, 2022) and the acidity may contribute to the natural selection of microorganisms during winemaking (Forino, Picariello, Rinaldi, Moio, & Gambuti, 2020). The pH value is directly involved in the definition of the equilibrium of sulfur dioxide in wine, affecting the amounts of free and molecular sulfur dioxide available (Morata, Gómez-Cordovés, Calderón, & Suárez, 2006). Indeed, pH and acidity are closely related to the solubility of tartaric salts (Comuzzo & Battistutta, 2018). The color of red wines can be strongly influenced by the pH value as it affects the balance among different forms of

anthocyanins (Kontoudakis, Esteruelas, Fort, Canals, & Zamora, 2011; Lapidot, Harel, Akiri, Granit, & Kanner, 1999; Sheridan & Elias, 2016). Finally, total acidity and pH have significant impacts on wine sensory perception (Forino et al., 2020; McRae, Kassara, Kennedy, Waters, & Smith, 2013; Miranda et al., 2020; Morata et al., 2006). In general, the monitoring of the acid fraction and pH is considered a minor technological issue in red winemaking. This is because red wines are commonly less acidic than whites and they often undergo malolactic fermentation during aging (Comuzzo & Battistutta, 2018). Nevertheless, this simplistic approach can lead to underestimating some important technological implications connected with pH management. Recently, climate changes and the pursuit of a wine style characterized by “sweet” tannins and color stability (to satisfy consumers’ expectations), determined the average increase of the pH of red wines compared with the values recorded some decades ago (Comuzzo & Battistutta, 2018). pH is also a key parameter to control beer aging and stability (Giménez-Gómez et al., 2017; Yang, Deed, Araujo, Waterhouse, & Kilmartin, 2022). From a sensory point of view, if the pH of fresh beer decreases below 4.00, the acute, acidic, bitter, and drying effects rapidly increase in intensity, with an enhanced metallic aftertaste for pH values below 3.70. Above 4.00, the effects on the palate refer to an increase of the scores for the biscuit and toasted characters, and even soapy and caustic notes if the pH exceeds 4.40 (Guyot-Declerck, Fran, Ritter, Govaerts, & Collin, 2005).

In the last three years, a robust pH colorimetric sensor array (CSA)

* Corresponding author.

E-mail address: paolo.pastore@unipd.it (P. Pastore).

<https://doi.org/10.1016/j.foodchem.2024.139513>

Received 22 November 2023; Received in revised form 28 March 2024; Accepted 27 April 2024

Available online 29 April 2024

0308-8146/© 2024 The Authors. Published by Elsevier Ltd. This is an open access article under the CC BY license (<http://creativecommons.org/licenses/by/4.0/>).

PVDF-supported (polyvinylidene fluoride) has been developed (Pastore, Badocco and Pastore, 2020b). From that starting point, the CSA was improved and adapted to specific applications. The key point was the modulation of the surfactant concentration present in the sensing spots which produced the continuous pKa variation of a single sensing indicator (Pastore, Badocco and Pastore, 2020a). All spots must be calibrated but only once as their calibration remains stable for a very long time (Pastore, Badocco and Pastore, 2020b). Some problems remained to obtain a reliable measurement such as the possibility to make the pH reading from the opposite side of the sensing membrane (Pastore, Badocco, & Pastore, 2022).

In the present paper, we will describe a novel compact device to detect the pH of wine and beer in the range of 2.50–6.50 based on a colorimetric detection method using H (hue, from the HSV color space) as the analytical signal. This CSA is characterized by reversibility and robustness. The signal reading is done from the opposite side of the sensing membrane contact with the solution. This CSA consists of i) a nitrocellulose membrane where various sensing spots are impregnated; ii) a CCD camera for the detection of the color; iii) an electronic board storing the calibration profiles of all spots in terms of Hue as a function of pH, and iv) a dedicated software to control the whole system and, v) a display to read the pH of the samples. To the best of our knowledge, this device represents the first CSA able to detect the pH in real-time even for slightly colored solutions. Various wines and beers will be tested. Specific buffers will be prepared to calibrate the sensor. The pH values read by the device will be compared with those obtained by the conventional glass electrode.

2. Materials, instrumentations, and procedures

2.1. Reagents and instrumentations

Bromocresol green (BCG), Hexadecyltrimethylammonium p-toluenesulfonate (CTApTs), tetraethyl orthosilicate (TEOS) ($\geq 99\%$), acetic acid, lactic acid, succinic acid, malic acid, citric acid, tartaric acid, and NaOH were provided by Sigma-Aldrich while ethanol and potassium sulfate from Carlo Erba. The nitrocellulose membrane sheets for immunoblotting (thickness $110.0 \pm 0.1 \mu\text{m}$; porosity of $0.45 \mu\text{m}$) were purchased from Goodfellow. The D65 LEDs were purchased from YUJILEDs (SAI 82 2 W LED SMD).

2.2. Preparation of nitrocellulose-supported colorimetric sensors

Two membranes were prepared for the experiments: **CSAsalt** and **CSAwine** (see Fig. 1(a,b)). The two CSAs are similar and were prepared to verify the CSA repeatability and to test if buffers prepared with different salts gave different responses.

CSAsalt consists of 11 spots and the **CSAwine** of 20 spots ($\varnothing \approx 3 \text{ mm}$ each). Each spot has a proper composition to work in a specific pH interval. Spots were deposited on the supporting membrane by using a steel bar. The membrane was glued to a plastic optical window with a commercial adhesive. All spots consist of a sol-gel solution prepared by acidic hydrolysis of TEOS (14.56 g of TEOS, 7.28 g of Milli-Q water, 0.21 g of HCl 1 M) containing specific surfactant concentration values, C_s . The amount of mixture used for one spot is $\approx 95 \mu\text{g}$.

The spots of **CSAsalt** contain BCG and CTApTs. The spots with concentrations of CTApTs, $C_s = 0, 0.51 \text{ M}$, were deposited in triplicate. The deposited solutions of BCG were prepared in ethanol by mixing

203.6 mg of the indicator with 13.55 g of EtOH. The C_s values decreased in the order 0.511 M (three times), 0.345, 0.234, 0.174, 0.118, 0.063, and 0 M (three times).

The spots of **CSAwine** contain BCG and CTApTs in two rows. The CTApTs concentration, C_s , decreased along the rows in the order: 0.511, 0.409, 0.353, 0.336, 0.325, 0.308, 0.295, 0.275, 0.254, 0.237, 0.226, 0.201, 0.168, 0.165, 0.143, 0.130, 0.122, 0.114, 0.104, 0.097 M. Both CSAs were left to age for three days. After the aging period, the CSAs are washed with a 0.08 M NaOH solution for 3 h to remove the unreacted chemicals and then left at $\text{pH} = 2$ for 2 days and then washed with water.

2.3. Preparation of the buffers for the calibration

The composition of the calibration buffers (reported in Table 1) was chosen by considering the mean conductivity of the real samples (750–1750 $\mu\text{S}/\text{cm}$) and close to the mean composition of red and white wines and beer (Coli, Rangel, Souza, Oliveira, & Chiaradia, 2015; Mongay, Pastor, & Olmos, 1996). The buffers were adjusted with suitable minimal amounts of HCl or NaOH leading to a substantially constant overall concentration of $\approx 0.053 \text{ M}$ in the presence of a total ethanol content of 12%. The working interval considered for the calibration of the CSA is in the range of 2.50–6.50 as the typical pH of white wines is between pH 3.00 and 3.50, for red wines is 3.40–4.00, and for beer, the interval is 3.70–5.00. pH values larger than 5.00 are recorded for beer sludges during the fermentation. During the sample's aging, acidification usually occurs leading to a pH variation. The same samples were tested in time to evaluate signal drift and other eventual anomalies.

2.4. Real samples

>20 real samples were tested. Here we report the case of three of them representative in terms of color of the solution and ethanol content. Sample 1 was a white wine (10.5% alcohol), sample 2 was a Prosecco (white wine, 11.6% alcohol) and sample 3 was a double malt beer (5.6% alcohol). The conductivity was between 800 and 1500 $\mu\text{S}/\text{cm}$.

2.5. Glass electrode and conductivity probe

The calibration of the Hanna Instruments HI11310 glass electrode was carried out at 16°C with two Hanna Instruments standard solutions at pH 7.00 and 4.01, respectively. The conductivity of the solutions was monitored with a conductivity probe HI763100 (Hanna Instruments).

2.6. CSA scheme

The compact device to detect pH is based on a colorimetric detection method with H (hue) from HSV color space as the analytical signal. The scheme of the measurement cell is reported in Fig. 2(a). This pH-meter consists of I) a colorimetric sensor array; II) D65 LEDs circularly arranged to guarantee constant lighting conditions; III) a CCD camera to perform the online detection of the color; IV) an electronic board with the calibration profiles of the Hue coordinate as a function of pH; and V) a display to read the pH of the samples.

Fig. 2(b) reports the various parts screwed together.

Table 1
Composition of the synthetic buffers used to calibrate the CSA (ethanol content 12% v/v).

Composition	pK_A	Concentration (M)
Acetic Acid	4.76	0.0110
Lactic Acid	3.86	0.0074
Succinic Acid	4.2; 5.6	0.0055
Malic Acid	3.4; 5.1	0.0065
Citric Acid	3.1; 4.8	0.0025
Tartaric Acid	3.0; 4.3	0.0139
Potassium Sulfate	strong; 1.99	0.0050

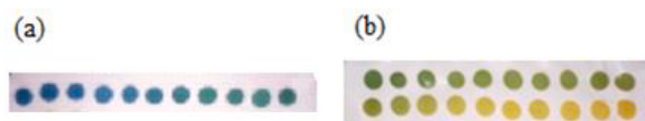


Fig. 1. (a) CSAsalt; (b) CSAwine.

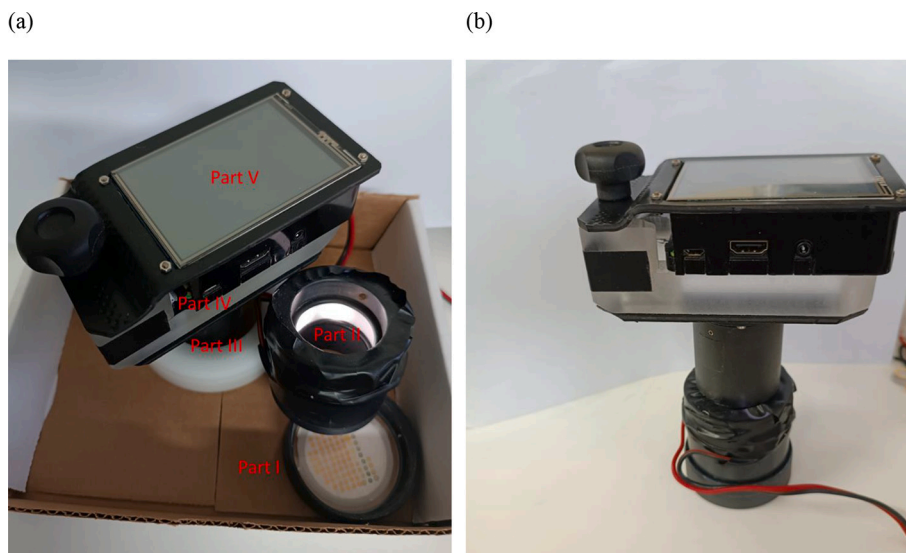


Fig. 2. (a) Scheme of the wireless compact device with the various components. The height is about 20 cm. The external diameter is about 6 cm while the internal one, corresponding to that of the nitrocellulose membrane housed on the bottom, is about 5 cm. (b) Measurement cell with the various components screwed together.

The device is powered by a battery and transmits data wireless to a remote computer. It is also equipped with a 2 W raspberry pi zero board keeping a record of the calibrations carried out once by the manufacturer. A dedicated software samples the images acquired in real-time and extrapolates the H coordinate in a spot area of a few hundred pixels. The median value of H for each spot is compared with that of its calibration and the final weighted pH value is returned.

2.7. Signal description

The shape of the H vs. pH profiles is sigmoidal, and it is fitted with the Boltzmann model (Pastore, Badocco, Cappellin, & Pastore, 2019). An example of the experimental sigmoidal profile of a single spot is reported in Fig. 3. The yellow, green, and blue circles characterize the color of the spot when it is immersed in an acidic (H_{Ind} species prevailing), intermediate (both H_{Ind} and Ind^- present, around the inflection point pH_i) and the basic solutions (Ind^- species prevailing), respectively.

The excursion of the signal of the spot is between $H = 0.120$ – 0.605 (Fig. 3 horizontal solid lines). A cut-off algorithm was used to define the window of H in which the spots can be considered active (dotted/dashed lines) cutting the 7% of both sides of the signal so that H varies between

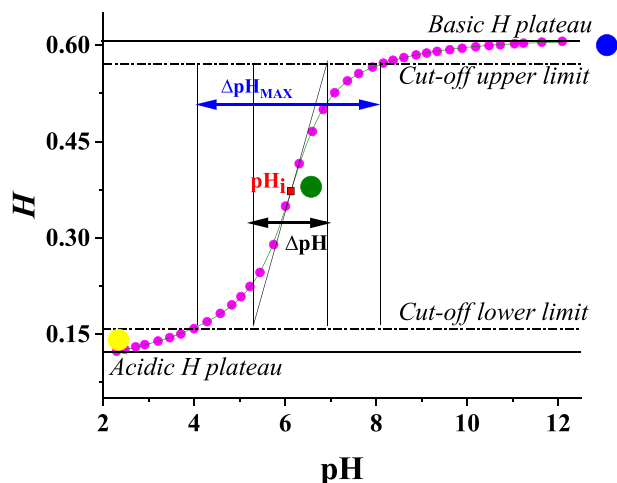


Fig. 3. Experimental sigmoidal profile of a spot.

0.153 and 0.572. ΔpH_{MAX} is, therefore, the working interval comprising 86% of the total excursion of the H signal, from the protonated form H_{Ind} to the deprotonated form Ind^- . ΔpH is the pH interval in which the calibration profile is essentially linear and characterized by an almost constant precision. pH_i is the pH of the inflection point and it is very close to the pK_a value (Pastore et al., 2022).

2.8. Calculation of the real sample pH: how each spot contributes to the final measurement

The H acquisitions were obtained after immersing the CSAs for 120 s. The color was sampled in a homogeneous central portion of the spot (≈ 800 pixels). Dedicated software was written and used to obtain the RGB coordinates (the median of 800 values for each spot), from which it was possible to calculate the HSV values and then the pH values. All regressions were run under MATLAB using the iterative “Levenberg Marquardt” algorithm (Mathematics, 2019). Each spot was characterized by a different calibration profile, i.e. a different working interval due to the different concentrations of surfactant contained in the spots. Each spot works in a specific interval so not all the spots work simultaneously. Their contribution ($pH_{read,i}$) to the mean pH value, \overline{pH} , (the output of the device) must be weighted for the slope and the regression variance obtained by the fitting of the calibration profile at the sample pH. The formula for the weight (w_i) is the following:

$$w_i = \frac{(1/s_{pH_i})^2}{\sum_i^N (1/s_{pH_i})^2}$$

Where s_{pH_i} is approximatively equal to the ratio $\frac{s_{y/x}}{b}$ where $s_{y/x}$ and b are the regression standard deviation and the slope of the calibration profile of the spot, respectively. The result reported by the display is therefore:

$$\overline{pH} = \sum_i^N (w_i \cdot pH_{read,i})$$

Where N is the number of working spots. The associated weighted standard deviation is:

$$\sqrt{\frac{\sum_i^N [w_i (pH_{read,i} - \overline{pH})^2]}{\frac{M-1}{M} \cdot \sum_i^N w_i}}$$

M is the number of non-zero weights (active spots). $\sum_i^N w_i$ is equal to 1 if all spots are considered. The pH reported on the display of the device is the median value obtained from 10 consecutive acquisitions of 1 s (10 values of \overline{pH}). The median of 10 values of the weighted standard deviation was determined accordingly.

3. Discussion

3.1. Supporting polymer choice

The use of the nitrocellulose membrane was optimal as its white color remained even in the presence of almost all colored matrices and the sample solution permeated the whole thickness allowing the correct color reading from the opposite side. Some problems are still present, at the actual state-of-the-art, in the case of red wine.

Initially, nylon and PVDF were tested as supporting membranes. With nylon, the spots impregnated the whole thickness, but the initially white color of the bare nylon membrane changed to yellow even with white wine and beer. PVDF was even worse for the purpose as the sample permeation through the sol was incomplete.

3.2. Calibration profiles and pH monitoring of fermented beverages

As the pH of white wine and beer ranges from 3.00 to 5.00, the CSA was prepared to monitor pH values from 2.50 to 6.50. Fig. 4(a) shows the calibration profiles of the 20 spots of CSAwine embedding BCG. The dotted-dashed lines indicate the cut-off window. The solid vertical lines indicate the pH of the samples. Fig. 4(b) represents the pH_i values vs. C_S for CSA_{salt} with the pH_i of the calibration (●) in Fig. 4(a) superimposed. In CSA_{salt}, three salinities (0.029 M, 0.061 M, and 0.397 M) were tested to quantify the shifts of the pH_i due to the competition of the anionic species. The buffers were prepared by using boric acid, phosphoric acid, and acetic acid. The total concentration of the first set of buffers is 0.029 M (equally distributed between the three acids). The following sets of buffers were prepared by adding to the 0.029 M solution an increasing amount of NaCl. Considering that the two CSAs are different and that they are used in completely different chemical environments (different temperatures, different anionic species in the

calibration buffer solutions, and different seasons) the robustness of the CSAs is very high. Indeed, the total buffer concentration is 0.053 M for CSA_{wine} vs. 0.061 M for CSA_{salt} suggesting that the salt effect depends on the concentration and not on the type of salts involved (Pastore et al., 2022).

In the next three tables, a 20-spot nitrocellulose-based CSA_{wine} has been tested for three different samples: a white wine (Table 2), prosecco (Table 3), and double malt beer (Table 4). In each table is reported the pH read by each spot, its weight, and the normalized hue values ($H = H/360$), the weighted standard deviation (SD), the pH value read by the glass electrode, the associated errors and, a picture of the sensor's spots during the measurement. The pH value read by the CSA is very similar to the one read by the glass electrode and the SD of the CSA is between 0.05 and 0.08 pH units. The surfactant concentration decreases from spot 1 to spot 20, so the H values decrease from spot 1 to 20 as expected. For a reason of simplicity, we reported only the parameters of the first 10 spots (characterized by larger weights). The number of active spots depends on pH. The active spots are 13 for samples 1 and 2 and 18 for sample 3. A cut-off algorithm has been used to define the window of the H signal in which the spots can be considered active. This adjustment is due to the exclusion of the portion of the sigmoidal profile where the sensitivity is quite low (the instrumental error of the camera is around $H = 0.005$ – 0.010). It can be noted that the H values increase in sample 3 since we move from $pH \approx 3.30$ to ≈ 4.30 . The spots with an H value close to 0.33–0.38 (near the pH_i) are the ones with the larger weight. For this reason, the most significant spots are 1 in the case of samples #1 and #2 and 2 and 3 in sample #3. The weight of the spots does not decrease linearly. For example, in samples 1 and 2, spot 3 has a lower weight than spot 4 even if H is larger. This is due to the inhomogeneity of the acquisition (an evident bubble in the nitrocellulose membrane). Spot 3 has a coherent weight in sample #3 since the bubble disappears (see CSA photo).

These results highlight how the calculation algorithm of pH acts as an efficient filter even in the presence of anomalous data, as demonstrated by the weighted pH value that is essentially the same that is measured by the glass electrode. The calibration of the membrane is maintained over time and works correctly also changing the chemical environment. The pH of sample 1 was also re-measured to monitor the acidification of the wine. For this purpose, the wine stopper was left half-open to simulate poor storage conditions. The next tables report the results obtained after ten days.

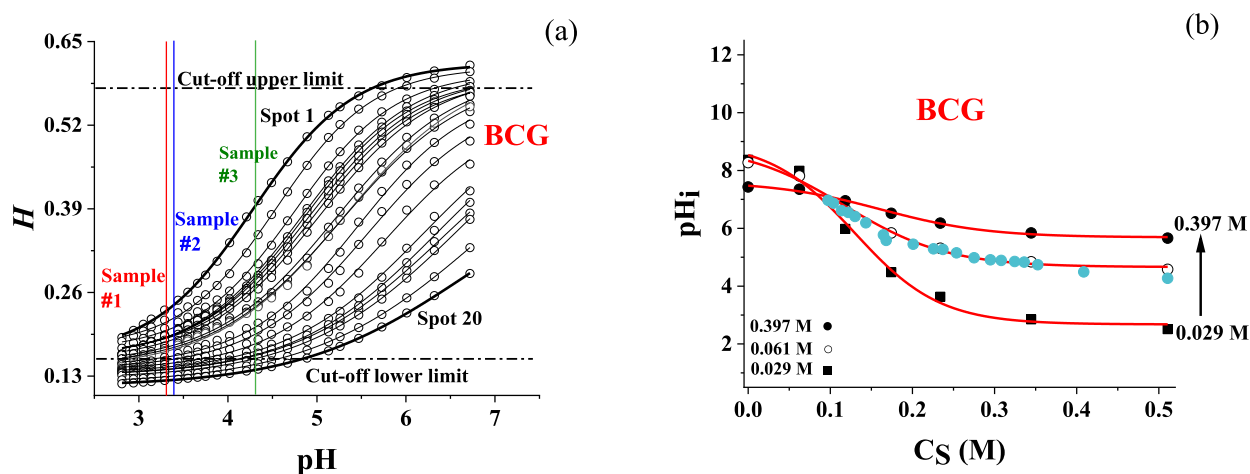


Fig. 4. (a) Calibration profiles of 20 spots of the CSA_{wine} in the wine-like buffer solutions. From spots 1 to 20, C_S decreases in the order reported in section 2.3. The dot lines indicate the cut-off window in which it is possible to consider a spot as “activated”. The solid vertical lines indicate the pH of the samples, and the rectangular selection indicates the values of the Hue of the spots at the pH of the sample. $T = 16^\circ\text{C}$. (b) pH_i values vs. C_S for CSA_{salt} for three levels of salinity 0.029 M (■), 0.061 M (○), and 0.397 M (●) with the pH_i of the calibration (●) in Fig. 4(a) superimposed.

Table 2

Sample #1 White wine, 10.5% (alcohol).


Spot position	pH read by the spot ($pH_{read,i}$)	Weight	Hue	pH_i ($\approx pK'_a$)	ΔpH_{MAX} (beginning and ending)
1	3.34	0.201	0.250	4.27	2.56–5.92
2	3.40	0.148	0.235	4.49	2.83–6.07
3	3.26	0.089	0.211	4.74	3.06–6.42
4	3.21	0.127	0.198	4.84	3.07–6.61
5	3.34	0.056	0.203	4.85	3.11–6.59
6	3.26	0.068	0.198	4.89	3.12–6.66
7	3.37	0.007	0.199	4.91	3.11–6.71
8	3.24	0.107	0.192	4.98	3.15–6.81
9	3.38	0.002	0.183	5.11	3.24–6.96
10	3.18	0.073	0.174	5.20	3.25–7.15
Weighted pH (CSA)	Weighted SD (CSA)	pH (glass electrode)	SD (glass electrode)	CSA photo	
3.30	0.08	3.31	0.02		

Table 3

Sample #2 Prosecco, 11.6% (alcohol).



Spot position	pH read by the spot ($pH_{read,i}$)	Weight	Hue	pH_i ($\approx pK'_a$)	ΔpH_{MAX} (beginning and ending)
1	3.31	0.193	0.247	4.27	2.56–5.92
2	3.33	0.134	0.229	4.49	2.83–6.07
3	3.44	0.106	0.222	4.74	3.06–6.42
4	3.29	0.123	0.203	4.84	3.07–6.61
5	3.39	0.062	0.207	4.85	3.11–6.59
6	3.26	0.070	0.198	4.89	3.12–6.66
7	3.42	0.009	0.203	4.91	3.11–6.71
8	3.28	0.107	0.194	4.98	3.15–6.81
9	3.52	0.003	0.189	5.11	3.24–6.96
10	3.39	0.073	0.186	5.20	3.25–7.15
Weighted pH (CSA)	Weighted SD (CSA)	pH (glass electrode)	SD (glass electrode)	CSA photo	
3.33	0.06	3.34	0.02		

Table 4

Sample #3 Double malt beer, 5.6% (alcohol).

Spot position	pH read by the spot ($pH_{read,i}$)	Weight	Hue	pH_i ($\approx pK'_a$)	ΔpH_{MAX} (beginning and ending)
1	4.20	0.118	0.399	4.27	2.56–5.92
2	4.26	0.152	0.356	4.49	2.83–6.07
3	4.31	0.152	0.324	4.74	3.06–6.42
4	4.28	0.147	0.299	4.84	3.07–6.61
5	4.31	0.064	0.299	4.85	3.11–6.59
6	4.29	0.087	0.284	4.89	3.12–6.66
7	4.27	0.011	0.292	4.91	3.11–6.71
8	4.29	0.100	0.277	4.98	3.15–6.81
9	4.40	0.005	0.269	5.11	3.24–6.96
10	4.48	0.067	0.267	5.20	3.25–7.15
Weighted pH (CSA)	Weighted SD (CSA)	pH (glass electrode)	SD (glass electrode)	CSA photo	
4.29	0.07	4.34	0.03		

3.3. Kinetic profiles

The t_{95} values (time required to reach 95% of the H plateau) for BCG spots in M1 vs. C_S are reported in Fig. 5 at 0.053 M buffer concentration. The empty circles indicate the t_{95} values referred to the transitions between $pH = 2.50$ and 6.50. The reverse transition is indicated with colored circles. The behavior in the two directions is not equal. The spots with larger C_S values are characterized by slower return times since the ion pair between the deprotonated form of the indicator and the cationic head of the surfactant represents an obstacle to the intake of the protons.

3.4. Attached video

In the short video attached (41 s), the CSAwine was immersed in sample #2 (Prosecco wine). The measured pH read by the CSA is 3.33. After 2 days, the pH value read by the device is still 3.33. In the video, the display shows the actual pH value joined to its weighted standard deviation (in parentheses). Even though the pH value is stable over time, the weighted standard deviation changes a little since it is influenced by external conditions (camera noise, light reflections, bubbles, etc.). On the second 27 (see Fig. 6), the display image switched to the real-time picture of the CSA. All the spots have a specific color. The black dots on each spot are software projections used by the algorithm to locate the

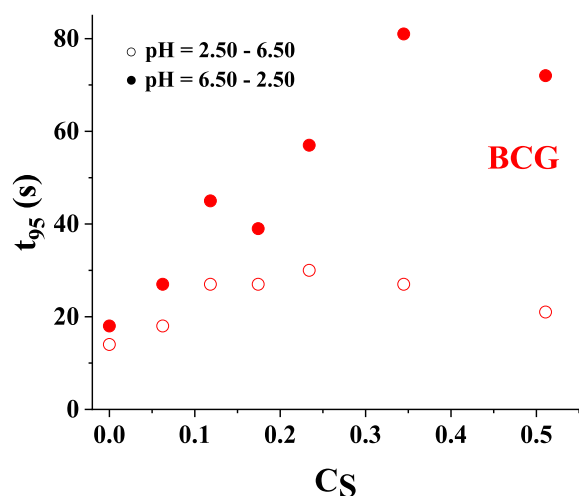


Fig. 5. t_{95} values (s) vs. C_s for M1. \circ indicates the t_{95} values referred to the transitions between pH = 2.50 and 6.50. The t_{95} values for the reverse pH transition are indicated with \bullet . Buffer concentration = 0.053 M. $T = 16^\circ\text{C}$.

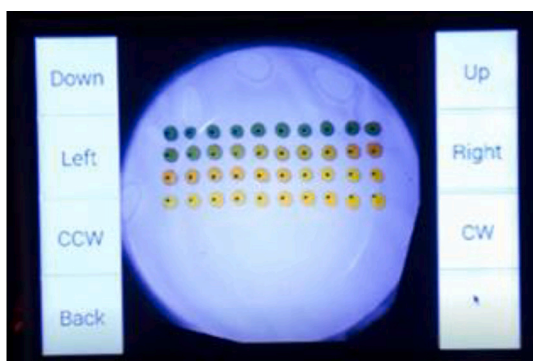


Fig. 6. Snapshot of the video at second 27.

color sampling position (the area inside each spot sampled for the color readings is 800 pixels).

4. Conclusions

A colorimetric sensor array (CSA) embedding Bromocresol green (BCG) has been successfully applied for the real-time monitoring of the pH of white wines and beer. A suitably prepared CSA was tested for three different samples (white wine, prosecco, and double malt beer) and the results were compared to those obtained with the glass electrode (CSA: $pH_{\text{wine}} = 3.30$, $pH_{\text{prosecco}} = 3.33$, $pH_{\text{beer}} = 4.29$; glass electrode: $pH_{\text{wine}} = 3.31$; $pH_{\text{prosecco}} = 3.34$; $pH_{\text{beer}} = 4.34$). Errors were comparable too, but the CSA has inherent advantages as it does not require recalibration, and, the read pH value remains stable in time indicating robustness and suggesting the use of the sensor for monitoring the pH of wine and beer even in barrels. The use of the nitrocellulose support was crucial as it allowed the color reading from the opposite side of the sample solution. The performance of the CSA was also compared with the performance of another CSA (CSAsalt) prepared with a similar composition. Considering that the two CSAs are different and that they are used in completely different chemical environments (different temperatures, different anionic species in the calibration buffer solutions, and different seasons) the robustness of the CSAs is high. At the actual state-of-the-art, in the case of red wine pH measurement, the color of the sample is a problem. For this reason, work is in progress to find suitable tricks to manage the pigment problem in red wine.

Supplementary data to this article can be found online at <https://doi.org/10.1016/j.foodchem.2024.139513>.

CRediT authorship contribution statement

Andrea Pastore: Writing – original draft, Methodology, Investigation, Data curation. **Denis Badocco:** Data curation, Conceptualization. **Luca Cappellin:** Supervision, Conceptualization. **Mauro Tubiana:** Data curation. **Paolo Pastore:** Writing – review & editing, Supervision.

Declaration of competing interest

The authors declare that they have no known competing financial interests or personal relationships that could have appeared to influence the work reported in this paper.

Data availability

Data will be made available on request.

References

- Belyustin, A. A., & Ivanovskaya, I. S. (2021). The glass electrode and electrode properties of glasses. In *I. Encyclopedia of glass science, technology, history, and culture* (pp. 609–617). <https://doi.org/10.1002/9781118801017.ch5.8>
- Cinquanta, L., De Stefano, G., Formato, D., Niro, S., & Panfilii, G. (2018). Effect of pH on malolactic fermentation in southern Italian wines. *European Food Research and Technology*, 244(7), 1261–1268. <https://doi.org/10.1007/s00217-018-3041-4>
- Coli, M. S., Rangel, A. G. P., Souza, E. S., Oliveira, M. F., & Chiaradia, A. C. N. (2015). Chloride concentration in red wines: Influence of terroir and grape type. *Food Science and Technology*, 35(1), 95–99. <https://doi.org/10.1590/1678-457X.6493>
- Comuzzo, P., & Battistutta, F. (2018). Acidification and pH control in red wines. In *Red wine technology*. Elsevier Inc.. <https://doi.org/10.1016/B978-0-12-814399-5.00002-5>
- Forino, M., Picariello, L., Rinaldi, A., Moio, L., & Gambuti, A. (2020). How must pH affects the level of red wine phenols. *Lwt*, 129(January), Article 109546. <https://doi.org/10.1016/j.lwt.2020.109546>
- Giménez-Gómez, P., Gutiérrez-Capitán, M., Capdevila, F., Puig-Pujol, A., Fernández-Sánchez, C., & Jiménez-Jorquera, C. (2016). Monitoring of malolactic fermentation in wine using an electrochemical bienzymatic biosensor for l-lactate with long term stability. *Analytica Chimica Acta*, 905, 126–133. <https://doi.org/10.1016/j.aca.2015.11.032>
- Giménez-Gómez, P., Gutiérrez-Capitán, M., Capdevila, F., Puig-Pujol, A., Fernández-Sánchez, C., & Jiménez-Jorquera, C. (2017). Robust L-malate bienzymatic biosensor to enable the on-site monitoring of malolactic fermentation of red wines. *Analytica Chimica Acta*, 954, 105–113. <https://doi.org/10.1016/j.aca.2016.11.061>
- Guyot-Declerck, C., Fran, N., Ritter, C., Govaerts, B., & Collin, S. (2005). Influence of pH and ageing on beer organoleptic properties. A sensory analysis based on AEDA data. *Food Quality and Preference*, 16(2), 157–162. <https://doi.org/10.1016/j.foodqual.2004.04.007>
- Kontoudakis, N., Esteruelas, M., Fort, F., Canals, J. M., & Zamora, F. (2011). Use of unripe grapes harvested during cluster thinning as a method for reducing alcohol content and pH of wine. *Australian Journal of Grape and Wine Research*, 17(2), 230–238. <https://doi.org/10.1111/j.1755-0238.2011.00142.x>
- Lapidot, T., Harel, S., Akiri, B., Granit, R., & Kanner, J. (1999). pH-dependent forms of red wine anthocyanins as antioxidants. *Journal of Agricultural and Food Chemistry*, 47(1), 67–70. <https://doi.org/10.1021/jf980704g>
- Magnaghi, L. R., Alberti, G., Zanoni, C., Guembe-Garcia, M., Quadrelli, P., & Biesuz, R. (2023). Chemometric-assisted litmus test: One single sensing platform adapted from 1–13 to narrow pH ranges. *Sensors*, 23(3), 10–16. <https://doi.org/10.3390/s23031696>
- Markoski, M. M., Garavaglia, J., Oliveira, A., Olivaes, J., & Marcadenti, A. (2016). Molecular properties of red wine compounds and cardiometabolic benefits. *Nutrition and Metabolic Insights*, 9, 51–57. <https://doi.org/10.4137/NMI.S32909>
- Mathematics, A. (2019). An algorithm for least-squares estimation of nonlinear parameters author (s): Donald W. Marquardt Source. *Journal of the Society for Industrial and Applied Mathematics*, 11(2), 431–441. Published by : Society for Industrial and Applied Mathematics S. 11(2).
- McRae, J. M., Kassara, S., Kennedy, J. A., Waters, E. J., & Smith, P. A. (2013). Effect of wine pH and bottle closure on tannins. *Journal of Agricultural and Food Chemistry*, 61(47), 11618–11627. <https://doi.org/10.1021/jf403704f>
- Miranda, K. W. E., Natarelli, C. V. L., Thomazi, A. C., Ferreira, G. M. D., Frota, M. M., do Bastos, M. S. R., ... Oliveira, J. E. (2020). Halochromic polystyrene nanofibers obtained by solution blow spinning for wine pH sensing. *Sensors (Switzerland)*, 20(2), 1–16. <https://doi.org/10.3390/s20020417>
- Mongay, C., Pastor, A., & Olmos, C. (1996). Determination of carboxylic acids and inorganic anions in wines by ion-exchange chromatography. *Journal of Chromatography A*, 736(1–2), 351–357. [https://doi.org/10.1016/0021-9673\(95\)01367-9](https://doi.org/10.1016/0021-9673(95)01367-9)

- Morata, A., Gómez-Cordovés, M. C., Calderón, F., & Suárez, J. A. (2006). Effects of pH, temperature and SO₂ on the formation of pyranoanthocyanins during red wine fermentation with two species of Saccharomyces. *International Journal of Food Microbiology*, 106(2), 123–129. <https://doi.org/10.1016/j.ijfoodmicro.2005.05.019>
- Pacheco, M., Winckler, P., Marin, A., Perrier-Cornet, J. M., & Coelho, C. (2022). Multispectral fluorescence sensitivity to acidic and polyphenolic changes in chardonnay wines - the case study of malolactic fermentation. *Food Chemistry*, 370 (October 2021), Article 131370. <https://doi.org/10.1016/j.foodchem.2021.131370>
- Pastore, A., Badocco, D., & Pastore, P. (2020a). Influence of surfactant chain length, counterion and OrMoSil precursors on reversibility and working interval of pH colorimetric sensors. *Talanta*, 212. <https://doi.org/10.1016/j.talanta.2020.120739>
- Pastore, A., Badocco, D., Cappellin, L., & Pastore, P. (2019). Enhancement of the pH measurement of a PVDF-supported colorimetric sensor by tailoring hue changes with the addition of a second dye. *Microchemical Journal*, 104552. <https://doi.org/10.1016/j.microc.2019.104552>
- Pastore, A., Badocco, D., & Pastore, P. (2020b). Reversible and high accuracy pH colorimetric sensor array based on a single acid-base indicator working in a wide pH interval. *Talanta*, 219(April), 1–7. <https://doi.org/10.1016/j.talanta.2020.121251>
- Pastore, A., Badocco, D., & Pastore, P. (2022). Determination of the relevant equilibrium constants working in pH colorimetric sensor arrays (CSAs). *Microchemical Journal*, 177(February), Article 107288. <https://doi.org/10.1016/j.microc.2022.107288>
- Salis, A., Pinna, M. C., Bilaničová, D., Monduzzi, M., Lo Nostro, P., & Ninham, B. W. (2006). Specific anion effects on glass electrode pH measurements of buffer solutions: Bulk and surface phenomena. *Journal of Physical Chemistry B*, 110(6), 2949–2956. <https://doi.org/10.1021/jp0546296>
- Sheridan, M. K., & Elias, R. J. (2016). Reaction of acetaldehyde with wine flavonoids in the presence of sulfur dioxide. *Journal of Agricultural and Food Chemistry*, 64(45), 8615–8624. <https://doi.org/10.1021/acs.jafc.6b03565>
- Stoica, D., Anes, B. V., Fiscaro, P., & Camões, M. F. (2021). Feasibility of multifunction calibration of H⁺-responsive glass electrodes in seawater (IUPAC technical report). *Pure and Applied Chemistry*, 93(12), 1487–1497. <https://doi.org/10.1515/pac-2020-0202>
- Yang, Y., Deed, R. C., Araujo, L. D., Waterhouse, A. L., & Kilmartin, P. A. (2022). Effect of microoxygenation on acetaldehyde, yeast and colour before and after malolactic fermentation on Pinot Noir wine. *Australian Journal of Grape and Wine Research*, 28 (1), 50–60. <https://doi.org/10.1111/ajgw.12512>